An Intercalated and Thermally Stable FAPY Adduct of Aflatoxin B_1 in a DNA Duplex: Structural Refinement from ^{1}H NMR†

Hui Mao,‡ Zhengwu Deng, Fang Wang, Thomas M. Harris, and Michael P. Stone*

Department of Chemistry and Center in Molecular Toxicology, Vanderbilt University, Nashville, Tennessee 37235

Received July 28, 1997; Revised Manuscript Received December 12, 1997

ABSTRACT: The structure of a formamidopyrimidine (FAPY) adduct arising from imidazole ring opening of the initially formed *trans*-8,9-dihydro-8-(N7-guanyl)-9-hydroxyaflatoxin B_1 adduct under basic conditions and positioned in the 5′-d(CTAT^{FAPY}GATTCA)-3′•5′-d(TGAATCATAG)-3′ oligodeoxynucleotide was determined. The FAPY adduct may be a major progenitor of aflatoxin B_1-induced mutations in DNA. The freshly prepared sample showed biphasic melting, with transitions at 28 and 56 °C. NMR initially showed multiple subspectra. Over a period of several days at 4 °C, the sample converted to a single species with a T_m of 56 °C, 15 °C greater than the unmodified duplex. The deoxyribose was in the β configuration about the anomeric carbon, evidenced by NOEs between ^{FAPY}G^5 H3′, H2′, H2″, and H1′. FAPY formation resulted in the loss of the guanine H8 proton, and the introduction of the formyl proton, which showed NOEs to ^{FAPY}G^5 H1′ and A^6 N6H$_a$. A total of 31 NOEs from AFB_1 to DNA protons were observed, mostly to the 5′-neighboring base, T^4 in the modified strand. Sequential NOEs were interrupted between T^4 and ^{FAPY}G^5 in the modified strand, between C^{16} and A^{17} in the complementary strand, and between T^4 N3H and ^{FAPY}G^5 N1H. An NOE between ^{FAPY}G^5 N1H and C^{16} N4H showed intact hydrogen bonding at ^{FAPY}G^5•C^{16}. Upfield chemical shifts were observed for T^4 H6 and A^{17} H8. Molecular dynamics calculations converged with pairwise rmsd differences of <0.9 Å. The sixth root residual was 8.7×10^{-2}. The AFB_1 moiety intercalated from the major groove between ^{FAPY}G^5 and T^4•A^{17}, and stacked with T^4 and ^{FAPY}G^5 and partially stacked with A^{17}. The base step between T^4•A^{17} and ^{FAPY}G^5•C^{16} was increased from 3.4 to 7 Å. The duplex unwound by about 15°. The FAPY formyl group was positioned to form a hydrogen bond with A^6 N6H$_a$. Strong stacking involving the AFB_1 moiety, and this hydrogen bond explains the thermal stabilization of four base pairs by this adduct, and may be a significant factor in its processing.

Aflatoxin B_1 (AFB_1)[1] is the predominant mutagenic fungal metabolite which is isolated from *Aspergillus flavus*, *parasiticus*, and *nomius*. This mycotoxin is of worldwide health concern because of the potential contamination of food (*1*). AFB_1 is a mutagen in several tester strains of bacteria (*2*); it is a hepatocarcinogen in experimental animals (*3, 4*). Epidemiological studies suggest that it causes cancer in humans (*3, 5, 6*). AFB_1 may be linked to site-specific transversions in the tumor suppression gene p53 (*7, 8*), and *ras* protooncogenes (*4, 9*).

AFB_1 is primarily metabolized in humans by cytochrome P_{450} 3A4 (*10*) to yield the ultimate carcinogen, AFB_1-*exo*-8,9-epoxide (*11*). This is one of the most reactive epoxides known with $t_{1/2}$ <1 s in H_2O (*12*). The regioselectivity of DNA adduction is consistent with a mechanism whereby precovalent intercalation on the 5′-face of guanine (*13*) places the epoxide in close proximity and in the proper orientation to the N7 position of guanine, thus facilitating a backside S_N2 reaction (*14*) to yield *trans*-8,9-dihydro-8-(N7-guanyl)-9-hydroxyaflatoxin B_1 (*15*).

† This work was supported by NIH Research Grants CA-55678 (M.P.S.) and ES-03755 (T.M.H.). The NMR was funded by NIH Instrumentation Grant RR-05805, and the Vanderbilt Center in Molecular Toxicology (ES-00267). The National Magnetic Resonance Facility at Madison was funded by the University of Wisconsin, NSF Grants DMB-8415048 and BIR-9214394, NIH Grants RR-02301, RR-02781, and RR08438, and the USDA. The Atlanta High Field NMR Facility at Georgia State University was funded by the State of Georgia and the NSF (BIR-9214443).

* To whom correspondence should be addressed. Phone: (615) 322-2589. FAX: (615) 322-4936. Email: stone@toxicology.mc.vanderbilt.edu.

‡ Present address: Frederik Philips Magnetic Resonance Research Center, Department of Radiology, Emory University School of Medicine, 1364 Clifton Rd. NE, Atlanta, GA 30322.

[1] Abbreviations: AFB_1, aflatoxin B_1; AFB_1−FAPY, AFB_1−formamidopyrimidine adduct; EDTA, ethylenediaminetetraacetic acid; FAPY, formamidopyrimidine; HPLC, high-pressure liquid chromatography; NMR, nuclear magnetic resonance; NOE, nuclear Overhauser enhancement; ppm, parts per million; DSS, sodium 4,4-dimethyl-4-silapentanesulfonate; STG, sterigmatocystin; TPPI, time proportional phase increment; TOCSY, total homonuclear correlated spectroscopy; 1D, one-dimensional; 2D, two-dimensional. The oligodeoxynucleotides discussed in this paper do not have terminal phosphate groups—we abbreviate the nomenclature for oligodeoxynucleotides by leaving out the phosphodiester linkage. A, C, G, T, and ^{FAPY}G refer to adenosine, thymidine, cytosine, guanosine, and the formamidopyrimidine rearrangement product of *trans*-8,9-dihydro-8-(N7-guanyl)-9-hydroxyaflatoxin B_1, respectively. A right superscript refers to the numerical position in the oligodeoxynucleotide sequence starting from the 5′-terminus of chain A and proceeding to the 3′-terminus of chain A and then from the 5′-terminus of chain B to the 3′-terminus of chain B. C2, C5, C6, C8, C1′, C2′, C2″, etc. represent specific carbon nuclei. H2, H5, H6, H8, H1′, H2′, H2″, etc. represent the protons attached to these carbons.

S0006-2960(97)01829-1 CCC: $15.00
Published on Web 03/11/1998

Scheme 1: Numbering Scheme for the FAPY-Modified Oligodeoxynucleotide

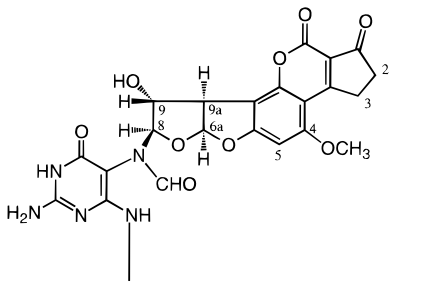

This cationic adduct undergoes base-catalyzed rearrangement to the *trans*-8,9-dihydro-8-(2,6-diamino-4-oxo-3,4-dihydropyrimid-5-yl formamido)-9-hydroxyaflatoxin B_1 (FAPY) derivative in which the imidazole ring has opened (*16*). The FAPY derivative is chemically stable, and is reported to be longer-lived than the initially formed cationic adduct (*17*, *18*). The FAPY adduct may be responsible for a significant fraction of AFB_1-induced mutations. Consequently, there has been considerable interest in understanding how the AFB_1−FAPY lesion perturbs duplex DNA. The related sterigmatocystin−FAPY lesion had the sterigmatocystin moiety intercalated on the 5′-side of the modified guanine, but a refined structure was not obtained (*19*).

This work presents a refined structure of an extraordinarily thermally stable AFB_1−FAPY adduct. The adduct is embedded in the oligodeoxynucleotide d(CTAT^{FAPY}GATTCA)• d(TGAATCATAG), as shown in Scheme 1. Structural refinement, using molecular dynamics restrained by NOE-based distances, shows that the stacking of the AFB_1 moiety above the 5′-face of the modified guanine results in unwinding of the DNA by approximately 15°. While the cationic adduct increased the stability of the DNA duplex slightly (*20*), in this oligodeoxynucleotide the FAPY adduct stabilizes four base pairs surrounding the lesion. Intercalation of the FAPY moiety occurs with little or no adduct-induced bending of this duplex, and maximum stacking interactions with the modified and 5′-neighbor base pairs. Moreover, refinement predicts the formation of a stabilizing hydrogen bond between the formyl group of the FAPY moiety and the exocyclic amino group of the 3′-neighbor adenine.

MATERIALS AND METHODS

Materials. Oligodeoxynucleotides were purchased from the Midland Certified Reagent Co. (Midland, TX). The purities were checked by HPLC, and SureCheck oligodeoxynucleotide analysis kits (Amersham Life Science). AFB_1 was purchased from Sigma−Aldrich Chemicals, Inc. (Milwaukee, WI). *Caution*: *Crystalline aflatoxins are hazardous due to their electrostatic nature and should be handled using appropriate containment procedures and respiratory mask to prevent inhalation. Aflatoxins can be destroyed by treatment with NaOCl. It should be assumed that aflatoxin epoxides are highly toxic and carcinogenic. Manipulations should be carried out in a well-ventilated hood with suitable containment procedures.* Dimethyldioxirane was prepared (*21*) and reacted with AFB_1 to give AFB_1-*exo*-8,9-epoxide (*11*).

Adduct Preparation. The reaction of 5′-d(CTATGATTCA)-3′•5′-d(AATCAT)-3′ with AFB_1-8,9-epoxide was carried out in a two-phase reaction system (CH_2Cl_2; 0.01 M sodium phosphate, 0.1 M NaCl, pH 7.0) for 5 min at 0 °C. The aqueous phase was transferred into pH 9.0 (uncalibrated reading) Na_2CO_3 buffer and stirred at 25 °C for 6 h. The AFB_1−FAPY-modified strand 5′-d(CTAT^{FAPY}GATTCA)-3′ was purified by HPLC on a YMC C18 reverse phase semi-prep column (ODS-AQ, 250 × 10 mm). The FAPY adduct eluted at 14.5 min at a flow rate of 4.0 mL/min with a gradient of 9−16% CH_3CN over 28 min in 0.01 M triethylammonium acetate (TEAA) buffer, pH 6.5. The AFB_1−FAPY adducted strand was digested enzymatically. The resulting FAPY nucleoside was compared with a standard from chemical synthesis and showed the correct mass spectrum of 613.2 for FAB^+ ($M + Na^+$).

NMR Samples. The oligodeoxynucleotide concentrations were determined from extinction coefficients of 9.81×10^4 M^{-1}•cm^{-1} for modified and 9.64×10^4 M^{-1}•cm^{-1} for the complementary strands, calculated at 260 nm (*22*). The complementary oligodeoxynucleotides were mixed at a 1:1 molar ratio. The mixture was heated to 65 °C for 5 min and was cooled to room temperature. The annealed duplex was lyophilized and redissolved in 0.5 mL of buffer solution containing 0.1 M NaCl, 10 mM NaH_2PO_4, and 50 μM Na_2-EDTA at pH 6.8. The solutions were lyophilized and exchanged 3 times with 99.96% D_2O. The strand concentrations of the samples were approximately 1.5 mM. The samples used for examining nonexchangeable protons were dissolved in 99.996% D_2O buffer. The samples used for the examination of the exchangeable protons were in buffer solution containing 9:1 H_2O/D_2O.

UV Melting. The experiments were carried out on a Varian Cary 4E spectrophotometer. The buffer was 10 mM sodium phosphate, 0.05 mM Na_2EDTA, and 1 M NaCl at pH 7.0. The buffer solution was degassed prior to the experiment. The concentrations were adjusted to 4.8×10^{-6} M in a 1 cm cuvette. The temperature was increased at a rate of 0.5 °C/min from 2 to 85 °C. Absorbance was measured at 260 nm. The melting temperatures of the native and modified oligodeoxynucleotides were calculated by determining the midpoints of the melting curves from the first-order derivatives.

NMR. NOESY and DQF−COSY experiments were performed at a ^1H frequency of 750.13 MHz. TOCSY and ROESY experiments were performed at a ^1H frequency of 500.13 MHz. The temperature was 25 °C. TMS was used to reference the spectra. Phase-sensitive NOESY spectra used in the resonance assignments were recorded using TPPI phase cycling with a mixing time of 350 ms. For examining exchangeable protons, phase-sensitive NOESY experiments were carried out in 9:1 H_2O/D_2O buffer at a ^1H frequency of 600 MHz. The field-gradient watergate pulse sequence suppressed the water signal (*23*). The spectra were recorded at 5 °C with a mixing time of 250 ms. Phase-sensitive TOCSY experiments were performed using a mixing time of 80 ms and MLEV17 spin lock pulse with TPPI phase cycling. To derive the distance restraints from NOESY experiments, three NOESY spectra were recorded consecutively at mixing times of 150, 250, and 350 ms, respectively. In these experiments, the data were recorded with 1024 real

data in the d1 dimension and 2048 real data in the d2 dimension. The data were processed using FELIX (Biosym Technologies) on Silicon Graphics Indigo^2 workstations. The data in the d1 dimension were zero-filled to give a matrix of 2K × 2K real points. A sinebell apodization function with a 90° phase-shift was used in both dimensions.

Structure Refinement. Footprints were drawn around the NOE cross-peaks for the NOESY spectrum measured at a mixing time of 350 ms to define the size and shape of the individual cross-peak using FELIX. The same set of footprints was applied to spectra measured at other mixing times. Cross-peak intensities were determined by volume integration of the areas under the footprints. The intensities were combined as necessary with intensities generated from complete relaxation matrix analysis of a starting DNA structure to generate a hybrid intensity matrix. MARDIGRAS (*24*) was used to iteratively refine the hybrid matrix to optimize the agreement with experimental NOE intensities.

Classical B-DNA and A-DNA (*25*, *26*) were used to create reference structures. The AFB_1 moiety was intercalated between T^4•A^{17} and G^5•C^{16} from the major groove side. The atomic charges of the AFB_1−FAPY nucleotide were assigned using MOPAC (*27*), and are collected in Table 4S and Figure 1S in the Supporting Information. The reference structures were energy-minimized for 500 iterations by the conjugate gradient method to give the starting structures used in MD calculations, FAPY−Bi and FAPY−Ai, respectively. Stereoviews of these are shown in Figure 2S in the Supporting Information. Calculations using DNA starting models generated by INSIGHTII, the three mixing time NOE experiments, and DNA correlation times of 2, 3, 4, and 5 ns yielded 12 sets of distance data. These data were pooled; average values of all minimum and maximum distances were used in setting error bounds to give the experimental NOE restraints used in subsequent molecular dynamics calculations (*28*).

Molecular Dynamics and Simulated Annealing. Potential energy minimization and restrained MD calculations were performed using X-PLOR (v. 2.4) (*29*) implemented with the CHARMM (*30*) force field. The empirical energy function (*31*) consisted of energy terms for bonds, bond angles, torsion angles, tetrahedral and planar geometry, hydrogen bonding, and nonbonded interactions including van der Waals and electrostatic forces. The van der Waals energy term was approximated using the Lennard−Jones potential energy function. The electrostatic term used the Coulomb function, based on a full set of partial charges (−1/residue). A distance-dependent dielectric constant of 4 was applied for all calculations. The nonbonded pair list was updated if any atom moved more than 0.5 Å, and a cutoff distance of 11 Å was used for the nonbonded interactions. The effective energy function was composed of two terms describing distance and dihedral restraints, which were in the form of a square well potential (*32*). All bond lengths involving hydrogen were kept fixed with the SHAKE algorithm (*33*) during MD calculations. The integration time step used in the molecular dynamics calculations was 1 fs. Structure coordinates were archived every 0.1 ps. All calculations were performed *in vacuo* without explicit counterions. Back-calculation of NMR data was performed using CORMA (*34*). The refined structure was analyzed using DIALS AND WINDOWS (*35*) to obtain the helicoidal parameters for both modified and unmodified oligonucleotides.

RESULTS

Thermal Stability. Thermal denaturing of a freshly prepared sample of the AFB_1−FAPY-modified duplex showed biphasic melting. The first transition occurred at 28 °C, and the second at 56 °C. A NOESY experiment performed ∼24 h after the modified oligodeoxynucleotide was prepared revealed multiple isomeric species. The sharp resonances for both conformations in the NMR spectra obtained shortly after the duplex sample was prepared, and the absence of exchange peaks, indicated that interconversion was slow on the NMR time scale. The initial conformation converted to a more stable form over a period of several days at 4 °C; eventually only the spectrum corresponding to the more stable conformation was observed. The rate of interconversion was not determined. The sample which had undergone conformational conversion for several days at 4 °C exhibited a single melting point at 56.0 °C, 15 °C higher than that of the native oligodeoxynucleotide. This paper describes refinement of the solution structure of the thermally stable conformation. At this juncture, the identity(ies) of the initially formed species remain(s) to be determined.

Nonexchangeable DNA Protons. The FAPY lesion interrupted the sequential NOE connectivities of B-form DNA at T^4, the nucleotide immediately 5′ to the adduct in the modified strand (Figure 1). For $^{FAPY}G^5$, opening of the guanine imidazole ring resulted in the loss of the guanine H8 proton, and the introduction of the $^{FAPY}G^5$ CHO proton, at δ 8.25 ppm. No sequential NOE was observed between T^4 H1′ or H2″, and $^{FAPY}G^5$ CHO. An intranucleotide NOE was observed between $^{FAPY}G^5$ CHO and $^{FAPY}G^5$ H1′. The normal intrastrand NOE connectivities resumed starting from $^{FAPY}G^5$ H1′→A^6 H8 and continued to the 3′-terminus. In the complementary strand, interruption of the sequential NOEs was observed between C^{16} H1′ or H2″, and A^{17} H8.

Corresponding interruptions of the sequential NOE connectivities between the base aromatic H6 or H8 protons were also observed. For the modified strand, these connectivities were interrupted at T^4 H6, which did not show an NOE to $^{FAPY}G^5$ CHO, and then resumed from A^6 H8 onward to the 3′-terminus. For the complementary strand, the sequential connectivities were interrupted at C^{16} H6, which did not show an NOE to A^{17} H8, and then resumed from A^{17} H8 to the 3′-terminus. At the nucleoside level, FAPY adduct formation was reported to result in rearrangement at the anomeric carbon from the β to the α configuration (*36*). The β configuration at C1′ was determined by unequivocally identifying the H2′ and H2″ resonances based upon NOE intensities to H3′, and subsequently comparing the intensities of NOEs between H2′ and H2″ to H1′ (Figure 2). The spectral assignments for both the FAPY-modified and unmodified oligodeoxynucleotide duplexes are summarized in Tables S1 and S2 in the Supporting Information.

Exchangeable Protons. The imino protons were assigned from NOE connectivities between adjacent base pairs and connectivities to the base-paired amino protons (*37*). Figure 3 shows NOE conectivities of exchangeable protons for the modified oligonucleotide. An interruption of the sequential imino-to-imino proton NOEs of adjacent base pairs was

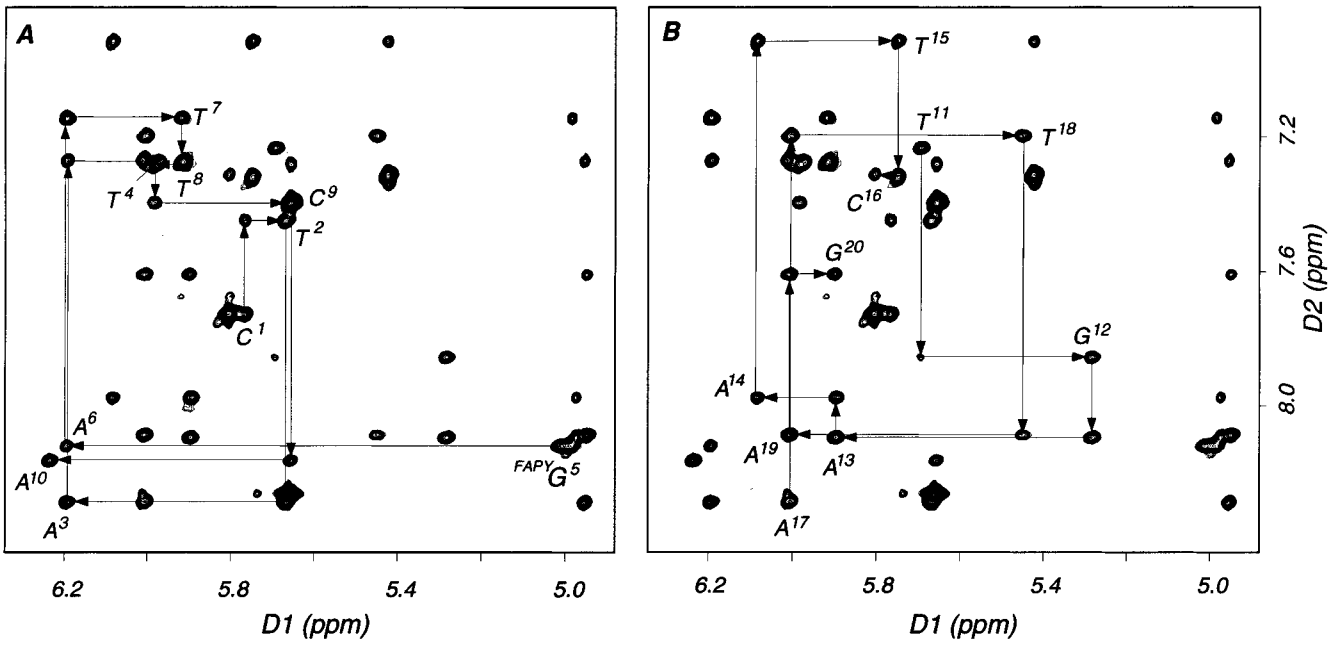

FIGURE 1: Expanded plots from the aromatic−anomeric region of the 750.13 MHz NOESY spectrum at 350 ms mixing time, showing sequential connectivities. (A) The modified strand. (B) The complementary strand.

found between T^4 N3H and $^{FAPY}G^5$ N1H. The strong cross-peaks between $^{FAPY}G^5$ N1H and C^{16} N4$H_{a,b}$ indicated that Watson−Crick hydrogen bonding between $^{FAPY}G^5$ and C^{16} was intact. Complete assignments of the exchangeable protons are listed in Table S3 in the Supporting Information.

AFB_1−FAPY Protons. The AFB_1 H5, H6a, H8, H9, H9a, and $-OCH_3$ resonances were assigned from NOE connectivities (Figure 4). AFB_1 H6a and H9a were identified from both COSY and NOESY experiments. H8 and H9 were assigned based on NOEs to H6a or H9a, and between themselves. A strong NOE from AFB_1 H5 to AFB_1 $-OCH_3$ revealed that that the latter resonance was at δ 3.52 ppm, while AFB_1 H5 was at δ 5.89 ppm. A new resonance at 8.25 ppm was observed, which was assigned as $^{FAPY}G^5$ CHO. This was suggested by NOEs to $^{FAPY}G^5$ H1′, and AFB_1 H6a and H8. A HMQC $^1H-^{13}C$ experiment verified a cross-peak between this proton and a carbon atom at δ 167 ppm, consistent with the formyl moiety. The assignment of the formyl proton was also supported by observing its cross-peak to AFB_1 H8 in the TOCSY spectrum. The methylene resonances from the cyclopentenone ring of AFB_1 were in the crowded deoxyribose H2′, H2″ region of the spectrum. NOE cross-peaks from the methylene protons $H2_\alpha$ and $H3_\beta$ were weak at all mixing times, possibly due to long relaxation times (*38*). Table 1 lists the assignments of the AFB_1 protons.

AFB_1−FAPY to DNA NOEs. A total of 31 NOEs from AFB_1 protons to DNA protons are listed in Table 2. The protons of the two AFB_1-fused furan rings showed NOEs to major groove and imino protons of the DNA; most of these were to the 5′-neighboring base-pair T^4•A^{17} (Figure 5). Thus, H6a and H9a, which were located on the same face of the AFB_1 moiety, both exhibited NOEs to T^4 H6 and CH_3. AFB_1 H8 and H9 exhibited similar NOEs, although in the case of H9, which was located on the opposite face of the AFB_1 moiety from H6a and H9a, the observed NOEs to T^4 could be due to spin diffusion. AFB_1 H9a showed an NOE to A^{17}

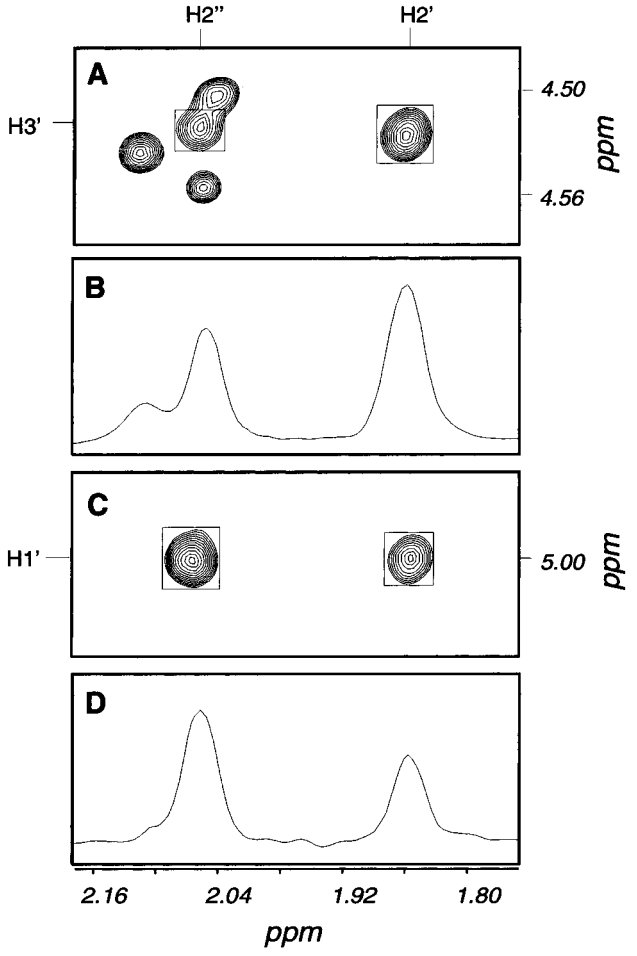

FIGURE 2: Expanded plots of a 750.13 MHz NOESY spectrum with mixing time 80 ms, at 25 °C, show (A) the cross-peaks from H3′ to H2′,H2″ and (B) their cross sections; (C) the cross-peaks from H1′ to H2′,H2″ and (D) their cross-sections.

NH_2 and T4 N3H. The AFB_1 H5 and $-OCH_3$ protons showed NOEs to a number of minor groove and imino DNA

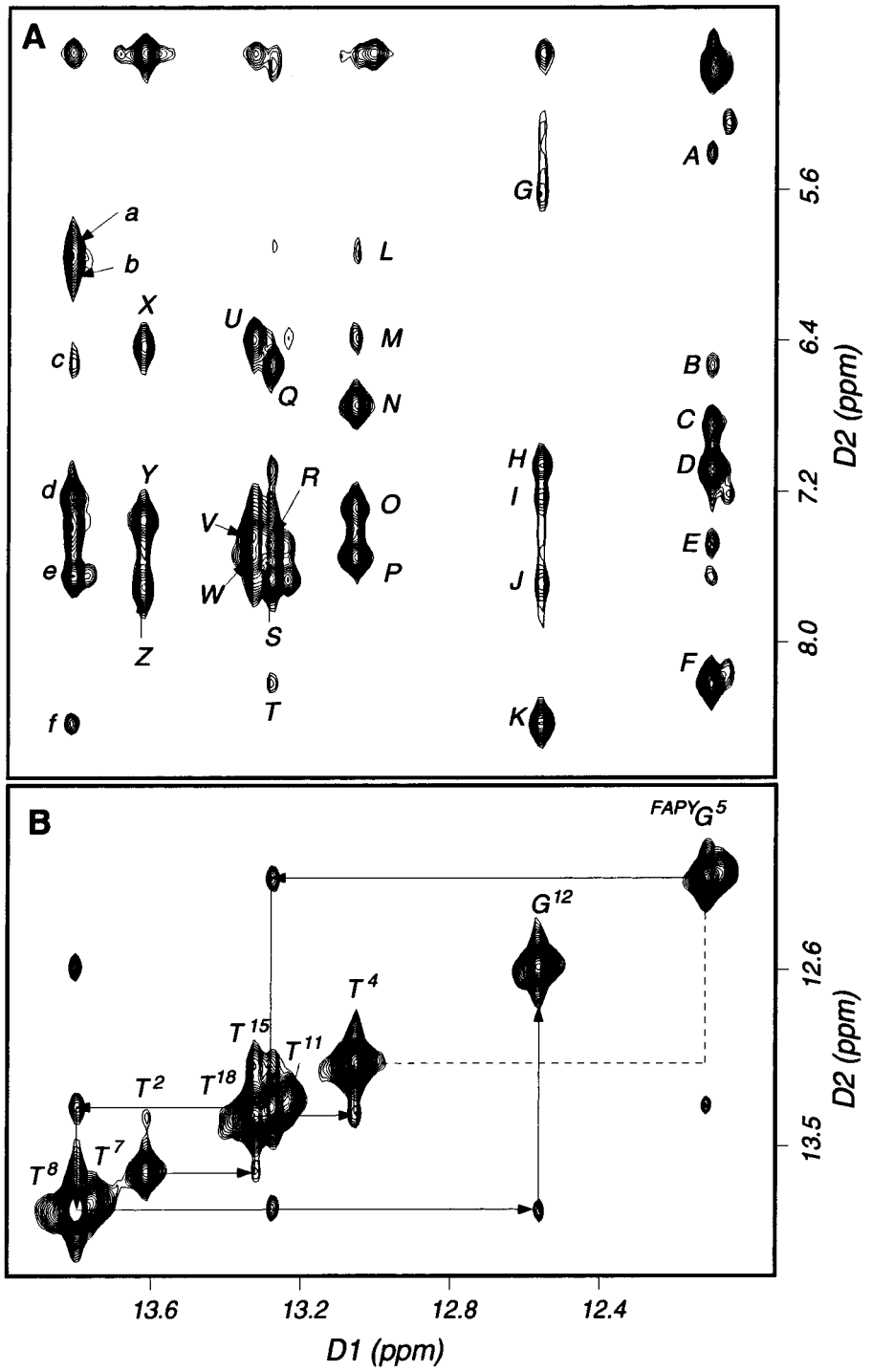

FIGURE 3: (A) Expanded plot showing the sequential NOE connectivities for the imino protons to the amino protons. The cross-peaks are assigned as (A) $^{FAPY}G^5$ N1H→C^{16} H5; (B) $^{FAPY}G^5$ N1H→A^6 N6H$_a$; (C) $^{FAPY}G^5$→C^{16} N4H$_a$; (D) $^{FAPY}G^5$ N1H→$^{FAPY}G^5$ N2H; (E) $^{FAPY}G^5$ N1H→A^6 N6H$_b$; (F) $^{FAPY}G^5$ N1H→C^{16} N4H$_b$; (G) G^{12} N1H→C^9 H5; (H) G^{12} N1H→C^9 N4H$_a$; (I) G^{12} N1H→A^{13} N6H$_a$; (J) G^{20} N1H→C^1 N4H$_b$; (K) G^{12} N1H→C^9 N4H$_b$; (L) T^4 N3H→$^{FAPY}G^5$ H6a; (M) T^4 N3H→A^3 N6H$_a$; (N) T^4 N3H→A^{17} N6H$_a$; (O) T^4 N3H→A^{17} H2; (P) T^4 N3H→A^{17} N6H$_b$; (Q) T^{15} N3H→A^6 N6H$_a$; (R) T^{15} N3H→A^6 N6H$_b$; (S) T^{15} N3H→A^6 H2; (T) T^{15} N3H→C^{16} N4H$_b$; (U) T^{18} N3H→A^3 N6H$_b$; (V) T^{18} N3H→A^3 H2; (W) T^{18} N3H→A^3 N6H$_b$; (X) T^2 N3H→A^{19} N6H$_a$; (Y) T^2 N3H→A^{19} H2; (Z) T^2 N3H→A^{19} N6H$_b$; (a) T^7 N3H→A^{14} N6H$_a$; (b) T^8 N3H→A^{13} N6H$_a$; (c) T^7 N3H→A^6 N6H$_a$; (d) T^8 N3H→A^{13} N6H$_b$; (e) $T^{7,8}$ N3H→$A^{13,14}$ H2; (f) T^8 N3H→C^9 N4H$_b$. (B) An expanded plot showing the sequential NOE connectivities for the imino protons. Dashed lines indicate interrupted NOE connectivities which were observed in the unmodified duplex. The data were collected at 600 MHz at 250 ms mixing time, at 5 °C.

protons. These were primarily to base pair T^4•A^{17}, in the 5′-direction, and the modified nucleotide $^{FAPY}G^5$. These included NOEs between AFB_1 −OCH_3 and T^4 H1′,H2′,H2″, $^{FAPY}G^5$ H1′, $^{FAPY}G^5$ NH_2, $^{FAPY}G^5$ N1H, and T^4 N3H. The cyclopentenone ring H_α and H_β protons exhibited NOEs to the minor groove H1′ proton of C^{16} in the complementary strand. There were no internucleotide NOEs observed between AFB_1 and the 3′-neighbor A^6•T^{15} base pair.

Chemical Shift Perturbations. The greatest effects were observed for the modified strand (Figure 6). In the major groove, T^4 H6 and CH_3 shifted downfield 0.15 and 0.3 ppm, respectively. In the minor groove, the deoxyribose protons

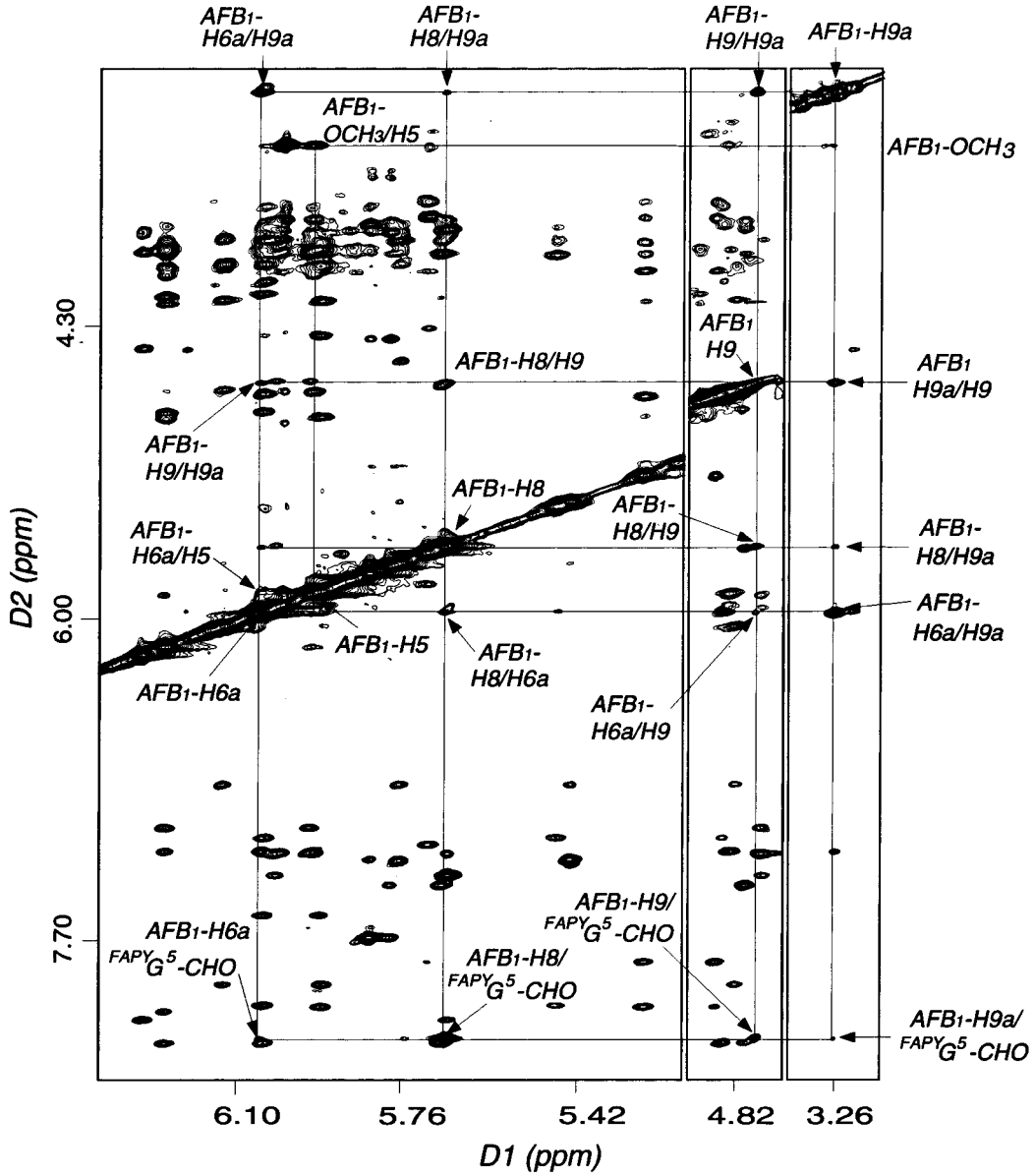

FIGURE 4: Tile plot of an expanded 750.13 MHz NOESY spectrum at 350 ms mixing time showing the assignments for the AFB_1 protons.

H1′, H2′, and H2″ were affected, at nucleotides T^4 and $^{FAPY}G^5$, and to a lesser extent, C^{16}. Examination of the exchangeable protons revealed that T^4 N3H at the 5′-side of $^{FAPY}G^5$ shifted ~0.6 ppm downfield. $^{FAPY}G^5$ N1H showed a smaller <0.2 ppm downfield shift. The C^{16} $N4H_a$ and $N4H_b$ amino protons shifted 0.3 and 0.2 ppm downfield, respectively. A^{17} $N6H_a$ shifted 0.2 ppm upfield. The amino proton A^6 $N6H_a$, at the 3′-side of the adduction site, displayed a 0.62 ppm downfield shift, while A^6 $N6H_b$ experienced <0.1 ppm chemical shift perturbation. T^7 N3H, two base pairs from the adducted site, experienced a 0.15 ppm downfield shift. With the exception of A^6 $N6H_a$, large chemical shift perturbations were not observed in the 3′-direction from the site of the lesion, at A^6•T^{15}.

Compared with AFB_1 (*39*) and the AFB_1−FAPY nucleoside,[2] the AFB_1 resonances showed upfield shifts in the oligodeoxynucleotide duplex (Table 1). As compared to the nucleoside, upfield shifts of 0.50 ppm for H5, 0.46 ppm for H6a, 0.65 ppm for H9a, and 0.41 ppm for $-OCH_3$ were observed. The exception was AFB_1 CHO which shifted 0.15 ppm downfield. The chemical shifts of the AFB_1 protons were also compared to the corresponding AFB_1 shifts in two cationic adducts previously examined, d(ATC^{AFB}GAT)•d(ATCGAT) and d(AT^{AFB}GCAT)$_2$ (*38*). With the exception of AFB_1 H5, the remaining AFB_1 protons were shifted substantially upfield as compared to the two cationic adducts.

NMR Melting Experiments. The thermal melting of the modified duplex was compared to the unmodified duplex by monitoring spectra of the imino protons as a function of temperature (Figure 7). For the modified duplex, at 65 °C, $^{FAPY}G^5$ N1H remained the sharpest signal in the imino region of the spectrum. Three additional broadened imino resonances were also observed at 65 °C, which were assigned as T^4 N3H of the 5′-neighbor base pair, T^{15} N3H of the 3′-neighbor base pair, and T^7 N3H. Thus, the presence of the FAPY lesion stabilized 4 base pairs, T^4•A^{17}, $^{FAPY}G^5$•C^{16}, A^6•T^{15}, and T^7•A^{14}, with regard to DNA melting. In contrast,

[2] R. S. Iyer, L. G. Iyer, M. W. Voehler, and T. M. Harris, manuscript in preparation.

Table 1: Chemical Shifts of the AFB_1−FAPY Protons in the Modified Oligodeoxynucleotide As Compared to the FAPY Nucleoside and Two *trans*-8,9-Dihydro[3]-8-(N7-guanyl)-9-hydroxyaflatoxin B_1 Adducts

proton	$AFB_{1,free}$[a] (ppm)	AFB_1−FAPY (ppm) (nucleoside)[b]	$\Delta\delta$ (ppm)[c]	AFB_1−FAPY (ppm) (oligonucleotide)	$\Delta\delta$ (ppm)[d]	$\Delta\delta$ (ppm)[e]	cationic adduct (ppm), d(ATC[AFB]GAT)• d(ATCGAT)[f]	$\delta\Delta$ (ppm)[g]	cationic adduct (ppm), d(AT[AFB]GCAT)$_2$[h]	$\delta\Delta$ (ppm)[i]
H5	6.69	6.39	−0.30	5.89	−0.80	−0.50	5.75	−0.94	5.80	−0.89
H6a	6.93	6.45	−0.48	5.99	−0.94	−0.46	6.75	−0.18	6.65	−0.28
H8[j]	6.59	6.27		5.63			6.37		6.26	
H9a	4.80	3.92	−0.88	3.27	−1.53	−0.65	3.93	−0.87	3.71	−1.09
H9[j]	5.57	4.92		5.97			6.07		5.98	
$-OCH_3$	3.98	3.93	−0.05	3.52	−0.46	−0.41	3.64	−0.34	3.81	−0.17
−CHO		8.10		8.25		0.15				
H3α	3.22	3.30		1.85	−1.37	−1.45	2.41	−0.81	2.22	−1.00
H3*β*	3.22	3.30		2.25	−0.97	−1.05	2.66	−0.56	2.73	−0.49
H2α	2.42	2.62		1.36	−1.06	−1.26	1.49	−0.93	1.51	−0.91
H2*β*	2.42	2.62		1.72	−0.70	−0.90	1.80	−0.62	1.94	−0.48

[a] From (*39*). [b] R. S. Iyer, L. G. Iyer, M. W. Voehler, and T. M. Harris, personal communication. [c] $\Delta\delta = \delta AFB_{1,\ FAPY(nucleoside)} - \delta AFB_{1,free}$. [d] $\Delta\delta = \delta AFB_{1,\ FAPY(oligonucleotide)} - \delta AFB_{1,free}$. [e] $\Delta\delta = \delta AFB_{1,\ FAPY(oligonucleotide)} - \delta AFB_{1,\ FAPY(nucleoside)}$. [f] From (*38*). [g] $\Delta\delta = \delta$d(ATC[AFB]GAT)•d(ATCGAT) $- \delta AFB_{1,free}$. [h] From (*38*). [i] $\Delta\delta = \delta$d(ATC[AFB]GAT)$_2 - \delta AFB_{1,free}$. [j] $\Delta\delta$ values are not provided for H8 and H9 since these change hybridization upon adduct formation.

Table 2: NOE Connectivities Observed between the Protons of the AFB_1−FAPY Lesion and DNA Protons

AFB_1−FAPY protons	DNA protons
H2α	C^{16} H1′
H3*β*	C^{16} H1′
H5	T^4 H6, T^4 H1′, T^4 H2′, T^4 H2″, $^{FAPY}G^5$ H5′
H6a	T^4 N3H, T^4 H6, T^4 H1′, T^4 H2′, T^4 H2″, T^4 H3′, T^4 CH_3
H8	T^4 H6, T^4 CH_3
H9a	T^4 H6, T^4 CH_3, A^{17}H2
H9	T^4 H6, T^4 CH_3
$-OCH_3$	T^4 H1′, T^4 H2′, T^4 H2″, $^{FAPY}G^5$ H5′, T^4 N3H, $A^{17}N6H_b$, $^{FAPY}G^5$ N1H, $^{FAPY}G^5$ NH_2
−CHO	$^{FAPY}G^5$ H1′, A^6 $N6H_a$

complete broadening of the imino protons occurred at 50 °C in the unmodified duplex.

Distance Restraints. A total of 549 restraints were derived from the NOESY experiments. In addition to the experimental restraints, 23 empirical distances based on hydrogen bonding geometries were applied. The final 572 interproton restraints consisted of 382 intranucleotide restraints, and 190 internucleotide restraints. A total of 26 of the 572 restraints were either intranucleotide or internucleotide AFB_1−FAPY to DNA restraints. Figure 8 summarizes the distribution of distance restraints among the nucleotides. The smaller number of distance restraints for some nucleotides, e.g., C^9, was generally due to overlapping resonances, preventing accurate measurement of cross-peak intensities. The nucleotides on both 5′- and 3′-termini yielded fewer internucleotide restraints.

Structural Refinement. Superposition of the six MD-generated structures for the AFB_1−FAPY-modified oligodeoxynucleotides from the FAPY−Ai family and the FAPY−Bi family is shown in Figure 9. The stick model shown in Figure 10 represents the final refined structure obtained by averaging 6 structures of ⟨rMD FAPY−Ai⟩ and six structures from ⟨rMD FAPY−Bi⟩ followed by 2000 steps of potential energy minimization using conjugate gradients. The overall structure maintained Watson−Crick base pairing. The AFB_1 moiety was intercalated from the major groove between $^{FAPY}G^5$ and T^4•A^{17}. Helicoidal analysis (*35*) revealed that the intercalated FAPY lesion unwound the modified duplex, and increased the base-step between T^4•A^{17} and $^{FAPY}G^5$•C^{16} to 7 Å (Figure 11). The adduct-induced unwinding was localized to the adducted base pair $^{FAPY}G^5$•C^{16} and its 5′- and 3′-neighbor base pairs T^4•A^{17} and A^6•T^{15}. The modified duplex was unwound approximately 15° at the adducted site, which was observed in the ribbon representation of the DNA phosphodiester backbone.

The structure refinement was evaluated for precision by comparing pairwise root-mean-square deviations (rmsd) of the individual structures to the average structure, tabulated in Table 3. That the final structures converged to a more B-like conformation was evidenced by the large rmsd between IniA and ⟨rMDA⟩ as compared to the smaller rmsd between IniB and ⟨rMDB⟩ . The rmsd calculations showed that both the FAPY−Ai and FAPY−Bi sets of calculations converged to common structures, independent of starting structure. Accuracy was evaluated by comparing the sixth root residuals between theoretical NOE intensities calculated for the emergent structures and the NMR data (Table 4). That the modified duplex more closely resembled the B-like starting structure was revealed by the improved R_1^x factor between the FAPY−Bi starting structure and the emergent average structure, as compared to the R_1^x factor between the FAPY−Ai starting structure and the emergent average structure. The refined set of structures ⟨MD FAPY−Bi⟩ starting from FAPY−Bi was slightly more accurate than the set ⟨MD FAPY−Ai⟩ derived from FAPY−Ai, but both were significantly improved as compared to the starting structures. The major improvement between the starting structures and the final refined structures was observed in the internucleotide NOEs, consistent with the expectation that intercalation and associated unwinding of the duplex perturbed the pattern of NOEs between adjacent base pairs, but not the intranucleotide NOEs. The final R_1^x value of ⟨rMDav⟩ of 8.7×10^{-2} suggested that the refined structures were in good agreement with the NOESY data.

DISCUSSION

Aflatoxin B_1, a mycotoxin and a strong environmental mutagen, is of concern due to its frequent contamination of

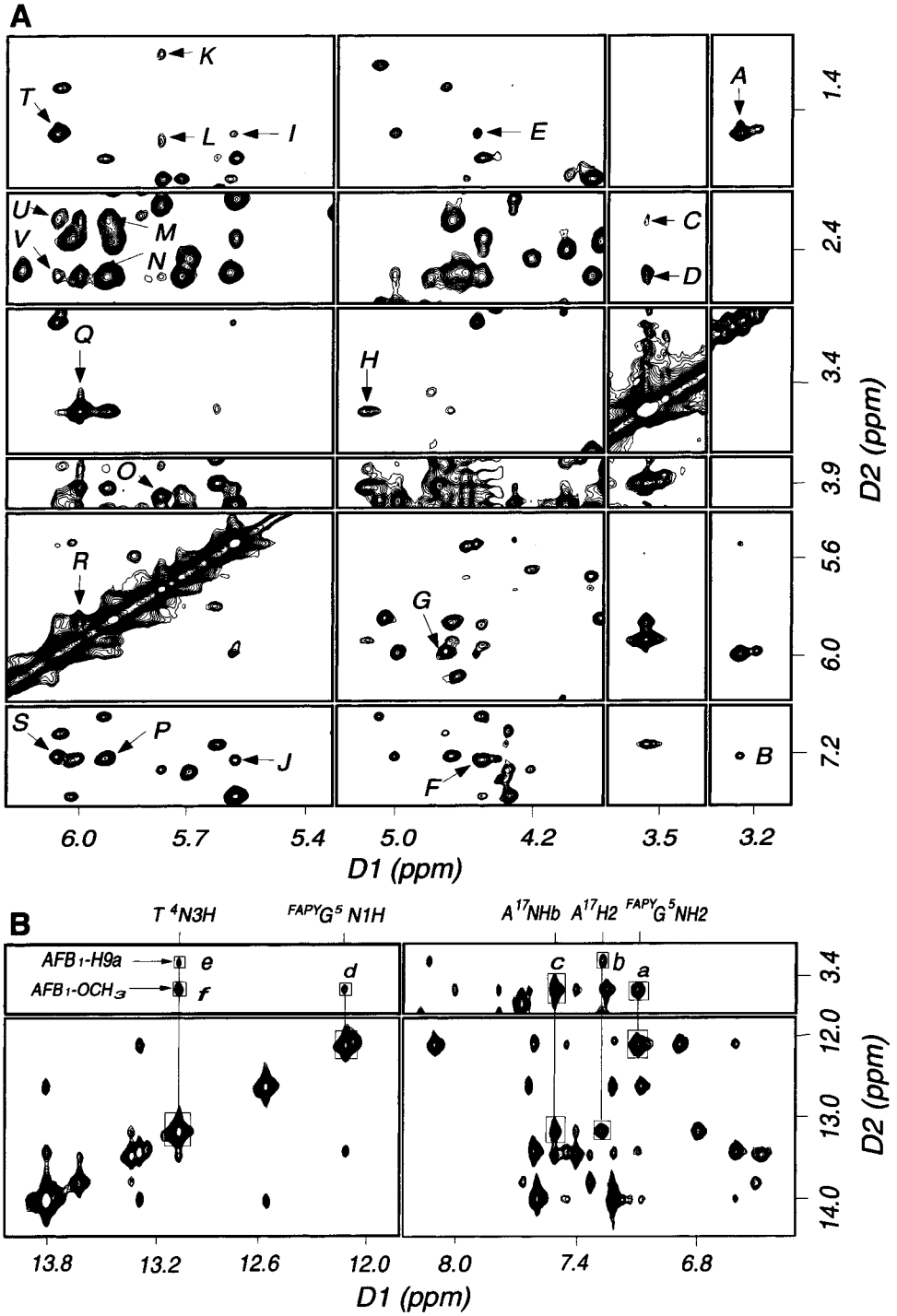

FIGURE 5: (A) Tile plot showing NOE cross-peaks between nonexchangeable protons of DNA and AFB_1 protons. (A) AFB_1 H9a→T^4 CH_3; (B) AFB_1 H9a→T^4 H6; (C) AFB_1 $-OCH_3$→T^4 H2′; (D) AFB_1 $-OCH_3$→T^4 H2″; (E) AFB_1 H9→T^4 CH_3; (F) AFB_1 H9→T^4 H6; (G) AFB_1 H6a→T^4 H3′; (H) AFB_1 $-OCH_3$→$^{FAPY}G^5$ H1′; (I) AFB_1 H8→T^4 CH_3; (J) AFB_1 H8→T^4 H6; (K) AFB_1 Hβ1→C^{16} H1′; (L) AFB_1 Hα2→C^{16} H1′; (M) AFB_1 H5→ $^{FAPY}G^5$ H5′; (N) AFB_1 H5→T^4 H2′; (O) AFB_1 H5→T^4 H2″; (P) AFB_1 H5→T^4 H6; (Q) AFB_1 $-OCH_3$→T^4 H1′; (R) AFB_1 H5→T^4 H1′; (S) AFB_1 H6a→T^4 H6; (T) AFB_1 H6a→T^4 CH_3; (U) AFB_1 H6a→T^4 H2′; (V) AFB_1 H6a→T^4 H2″. (B) Tile plot showing NOE cross-peaks between exchangeable protons of DNA and AFB_1 protons. (a) AFB_1 $-OCH_3$→$^{FAPY}G^5$ NH_2; (b) AFB_1 H9a→A^{17} NH_2; (c) AFB_1 $-OCH_3$→A^{17} H2; (d) AFB_1 $-OCH_3$→$^{FAPY}G^5$ N1H; (e) AFB_1 H9a→T^4 N3H; (f) AFB_1 $-OCH_3$→T^4 N3H.

a variety of economically important agricultural products. Two cationic guanine N7 adducts of AFB_1, d(ATC^{AFB}-GAT)•d(ATCGAT) and d(AT^{AFB}GCAT)$_2$, intercalated above the 5′-face of the modified guanines (*38*). A cationic guanine N7 adduct of sterigmatocystin intercalated in a similar manner (*40*). Subsequently, site-specific mutagenesis experiments revealed that the cationic AFB_1 adduct induced mutations at the lesion site, and in the 5′-direction from the lesion site, an observation consistent with the structural studies (*41*). The present structural study was motivated by the general observation that adducts at guanine N7 are susceptible to base-catalyzed conversion to the corresponding imidazole-ring-opened FAPY adducts. In the case of AFB_1, the chemical stability of the AFB_1−FAPY lesion, and its reported long half-life (*17, 18*), suggested that it could be a major progenitor of AFB_1-induced mutations. Hence, the

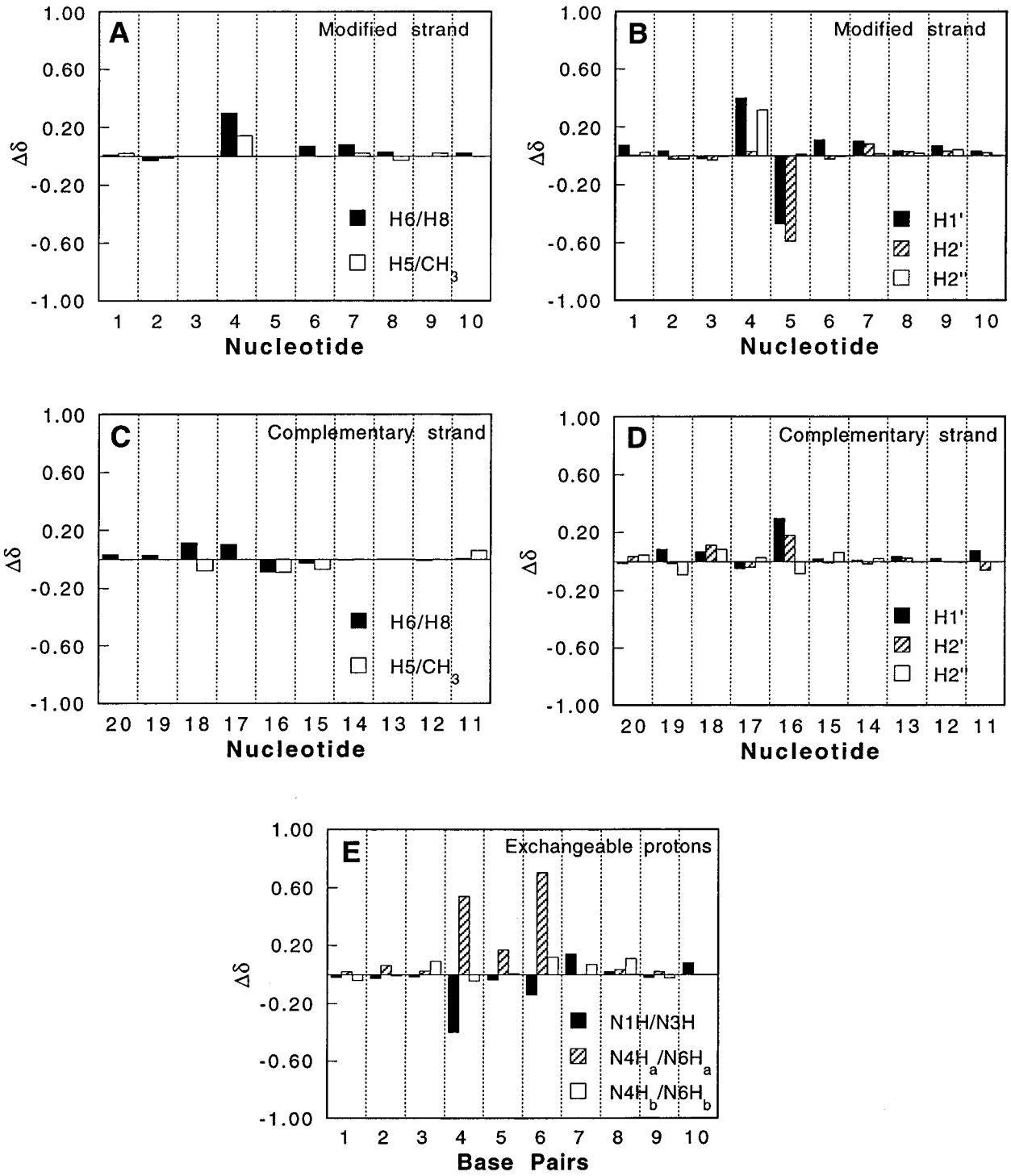

FIGURE 6: Chemical shift changes of selected protons relative to the unmodified oligodeoxynucleotide duplex. (A) Major groove protons in the modified strand. (B) Minor groove protons in the modified strand. (C) Major groove protons in the complementary strand. (D) Minor groove protons in the complementary strand. (E) Exchangeable imino and amino protons. $\Delta\delta = [\delta_{\text{unmodified oligodeoxynucleotide}} - \delta_{\text{modified oligodeoxynucleotide}}]$ (ppm).

structure and mutagenic properties of the AFB_1−FAPY adduct are of considerable interest.

The AFB_1−FAPY Adduct. The approach to this site-specific FAPY−AFB_1 adduct involved reaction of the duplex oligodeoxynucleotide containing a single guanine in the target strand with AFB_1 epoxide (*11, 20*). There were initial concerns that the FAPY adduct would exist as multiple species, complicating both the isolation and subsequent spectroscopy. At the nucleoside level, NMR studies of other FAPY adducts (*42, 43*) indicated the presence of rotational isomers about the C5−N5 bond of the pyrimidine moiety. A study of the sterigmatocystin−FAPY adduct at the oligodeoxynucleotide level advanced a similar hypothesis (*19*). Alternatively, the potential for interconversion between the β and α configurations at the anomeric carbon existed (*36*).

Despite these concerns, the previous study of the sterigmatocystin−FAPY adduct at the oligodeoxynucleotide level (*19*) reported that while a mixture of species initially formed, these subsequently rearranged with a half-life of several days

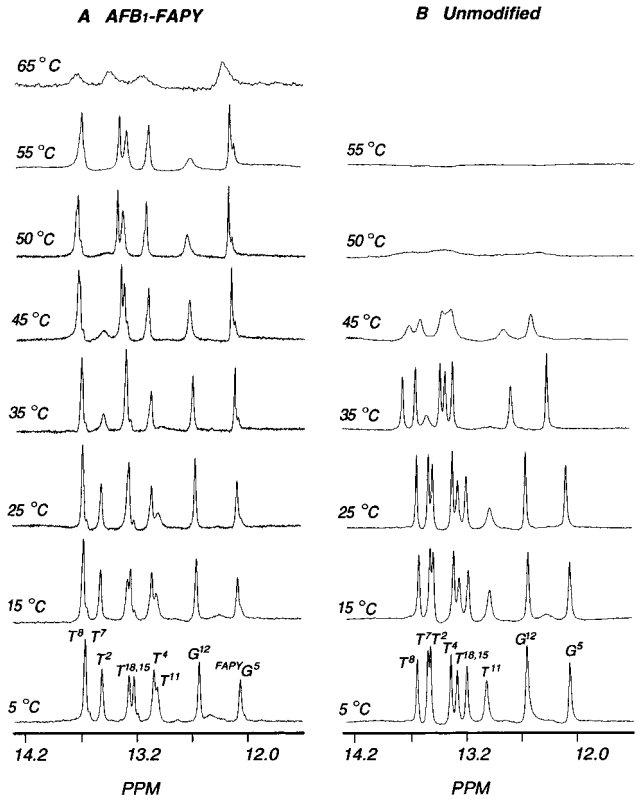

FIGURE 7: Expanded spectra of imino protons of (A) the modified and (B) the unmodified oligonucleotides as a function of temperature.

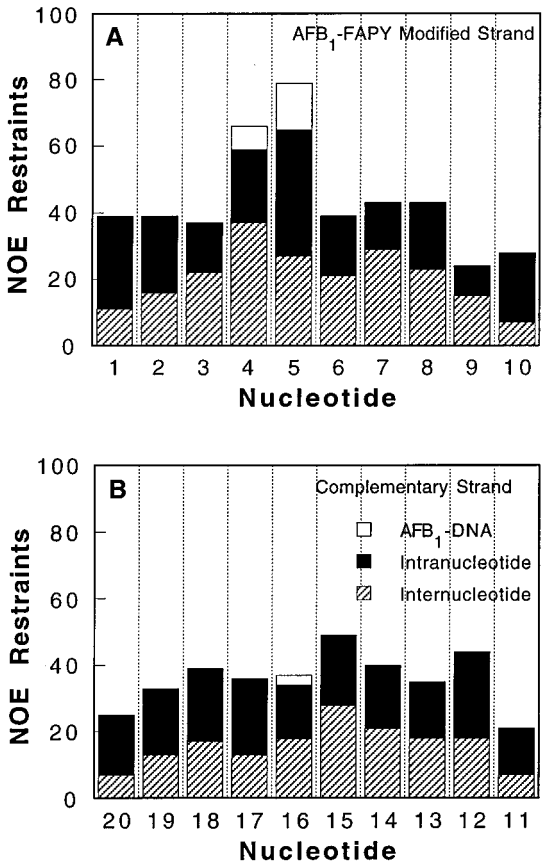

FIGURE 8: Distribution of NOE restraints applied in the structural refinement. (A) AFB_1−FAPY-modified strand. (B) Complementary strand.

to a homogeneous sample. It was concluded that for the stable species, the sterigmatocystin chromophore was intercalated 5′ to the modifed guanine, with the chromophore spanning the helix. Our work revealed that the AFB_1−FAPY adduct behaved similarly, with regard to the rearrangement over a time period of several days to a homogeneous sample, and the general features of the 5′-intercalated AFB_1 chromophore. Significantly, the present work revealed the extraordinary thermal stability of the AFB_1−FAPY lesion in this DNA sequence. The stacking patterns and potential hydrogen bonding interactions which may provide a basis for this unusual thermal stability emerged from a detailed structural study.

Structure of the AFB_1−FAPY Lesion. Figure 12 shows stacking patterns calculated for the AFB_1−FAPY-modified oligomer, as compared to the corresponding unmodified oligomer. The intercalated aflatoxin moiety stacked with the T^4 and $^{FAPY}G^5$ pyrimidine rings in the modified strand and partially stacked with C^{16} and A^{17} in the complementary strand. This was consistent with the pattern of NOEs in the 5′-direction from the AFB_1 moiety to base pair T^4•A^{17}. As in the cationic adduct (*38*), NOEs between AFB_1 H6a and H9a, located at the juncture of the two furan rings, to T^4 H6 and CH_3 provided diagnostic markers of the 5′-orientation of the aflatoxin moiety. The NOEs from AFB_1 H6a, H8, H9, and H9a to major groove protons, from AFB_1 $-OCH_3$ to T^4 and $^{FAPY}G^5$ deoxyribose protons, in the minor groove, and the cross-strand NOEs from the AFB_1 cyclopentenone ring to C^{16} H1′, also in the minor groove, provided strong evidence that AFB_1 spanned the helix.

The interruptions of sequential NOE connectivities between base pairs T^4•A^{17} and $^{FAPY}G^5$•C^{16} provided further support of the notion that the AFB_1 moiety was intercalated between these two base pairs. No sequential NOE was observed between T^4 H1′ or H2″, and $^{FAPY}G^5$ CHO. An intranucleotide NOE was observed between $^{FAPY}G^5$ CHO and $^{FAPY}G^5$ H1′. The normal intrastrand NOE connectivities resumed starting from $^{FAPY}G^5$ H1′→A^6 H8 and continued to the 3′-terminus. In the complementary strand, interruption of the sequential NOEs was observed between C^{16} H1′ or H2″, and A^{17} H8. Corresponding interruptions of the sequential NOE connectivities between the base aromatic H6 or H8 protons were also observed. For the modified strand, these connectivities were interrupted at T^4 H6, which did not show an NOE to $^{FAPY}G^5$ CHO, and then resumed from A^6 H8 onward to the 3′-terminus. For the complementary strand, the sequential connectivities were interrupted at C^{16} H6 and H1′, which did not show NOEs to A^{17} H8, and then resumed from A^{17} H8 to the 3′-terminus. An interruption of the sequential imino-to-imino proton NOEs of adjacent base pairs was found between T^4 N3H and $^{FAPY}G^5$ N1H. The strong cross-peaks between $^{FAPY}G^5$ N1H and C^{16} $N4H_{a,b}$ indicated that Watson−Crick hydrogen bonding between $^{FAPY}G^5$ and C^{16} was intact.

Unusual Stability of the FAPY Lesion. A striking feature of this AFB_1−FAPY adduct was the 15 °C increase in T_m for the modified duplex, as compared to the parent duplex. In comparison, the cationic lesions stabilized the d(ATC^{AFB}-GAT)•d(ATCGAT) and d(AT^{AFB}GCAT)$_2$ duplexes by 3−5 °C (*20, 38*), which was attributed to the formation of stacking interactions between the AFB_1 moiety and the adjacent base pairs. To our knowledge, with the exception of cross-linking

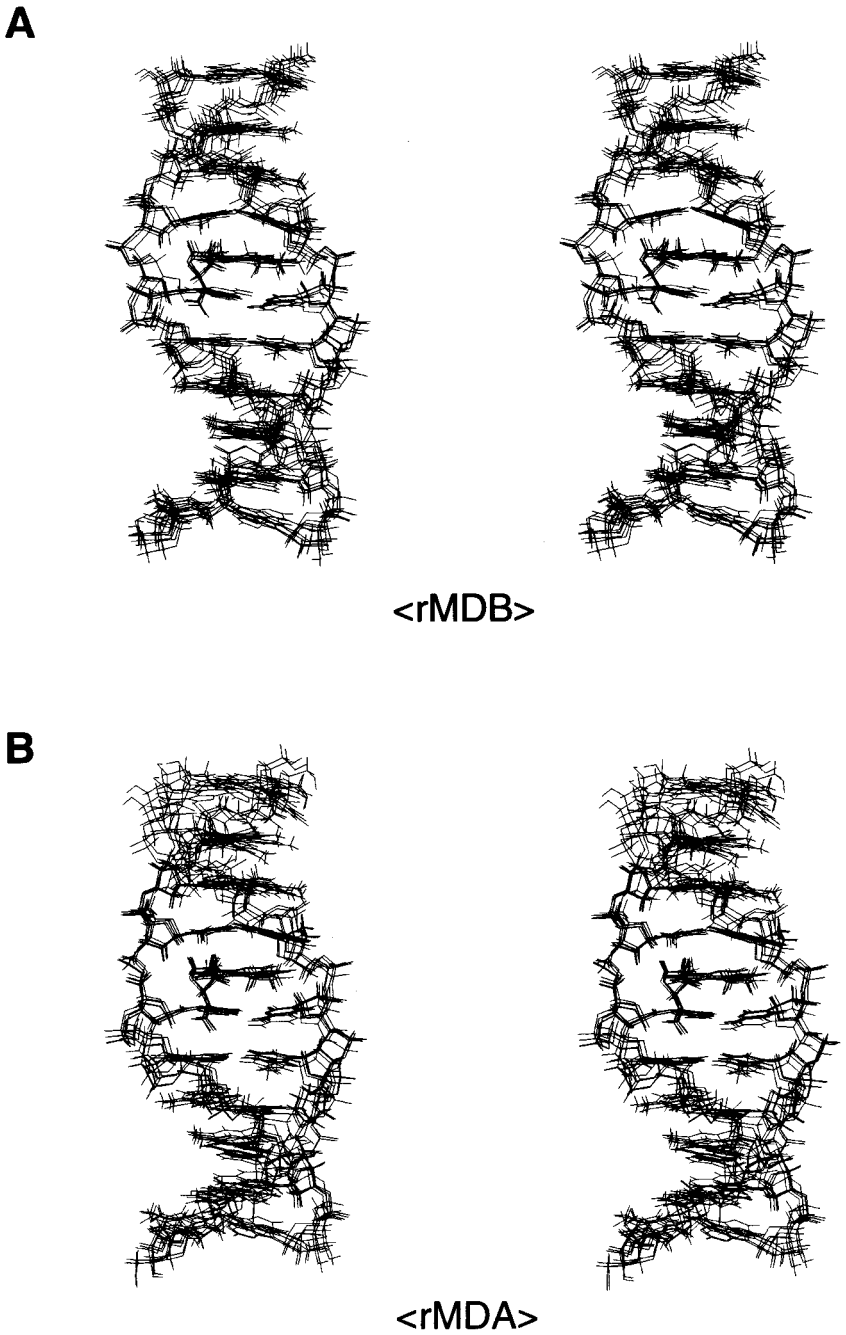

FIGURE 9: Stereoviews showing the comparisons of (A) six superimposed ⟨rMDFAPY−Bi⟩ structures and (B) six superimposed ⟨rMDFAPY−Ai⟩ structures.

agents, these aflatoxin adducts are thus far unique in increasing the thermal stability of the DNA duplex. The present structure suggests that stacking interactions are enhanced in the FAPY lesion, since ring opening of the imidazole allows the AFB_1 to intercalate approximately parallel to the DNA base pairs, and with minimal helical bending. The AFB_1 moiety was approximately parallel to base pairs T^4•C^{17} and $^{FAPY}G^5$•C^{16}, although the refined structures predicted a downward buckling of base pair $^{FAPY}G^5$•C^{16}.

The predicted hydrogen bond between the formyl group of the pyrimidine moiety and A^6 $N6H_a$ of the base pair A^6•T^{15} provides an additional potential source of thermal stability. The calculated distance between the formyl oxygen and A^6 N6 was 2.68 Å, and the calculated angle O•••H−N was 130°. Only one resonance signal was observed for $^{FAPY}G^5$ CHO, which suggested that rotation about the formyl bond was restrained in duplex DNA. The 0.6 ppm downfield shift of A^6 $N6H_a$ was consistent with redistribution of the electron density from the formyl oxygen to A^6 $N6H_a$. The NOE observed from the $^{FAPY}G^5$ formyl proton to A^6 $N6H_a$ also suggested that the two protons were in proximity.

The thermal stability of this FAPY adduct was also evident in the NMR spectra of the Watson−Crick imino resonances as a function of temperature (Figure 7). For the modified duplex, at 65 °C, $^{FAPY}G^5$ N1H remained the sharpest signal in the imino region of the spectrum. Three additional broadened imino resonances were also observed 65 °C, which were assigned as T^4 N3H, of the 5′-neighbor base pair, T^{15} N3H, of the 3′-neighbor base pair, and T^7 N3H. Thus, the presence of the FAPY lesion stabilized 4 base pairs with regard to DNA melting, T^4•A^{17}, $^{FAPY}G^5$•C^{16}, A^6•T^{15}, and

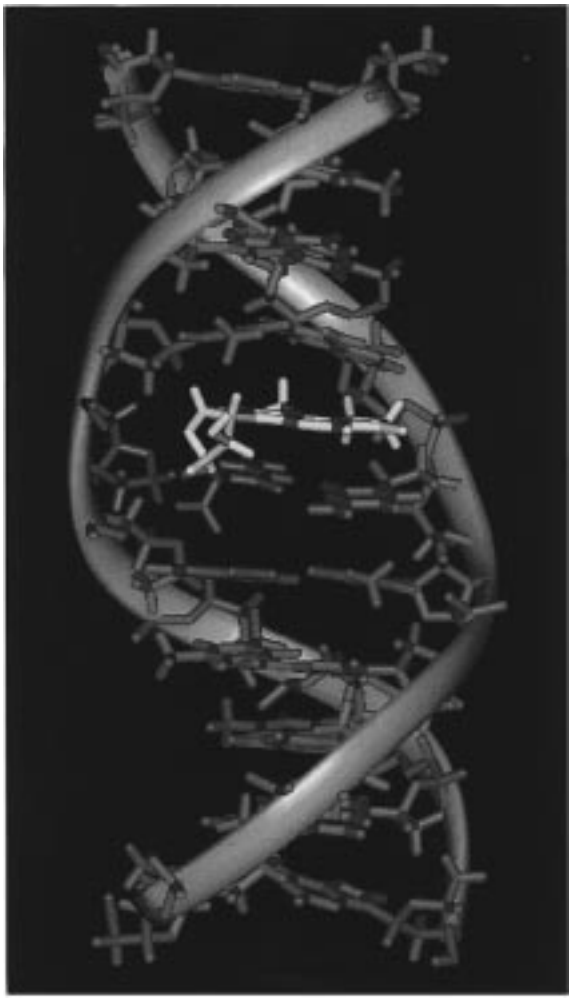

FIGURE 10: Stick-ribbon model representation of the final structure of AFB_1−FAPY-modified oligodeoxynucleotide, ⟨rMDav⟩, averaged from the 12 sets of 2 families of rMD structures, ⟨rMDA⟩ and ⟨rMDB⟩. The AFB_1 moiety is colored in yellow.

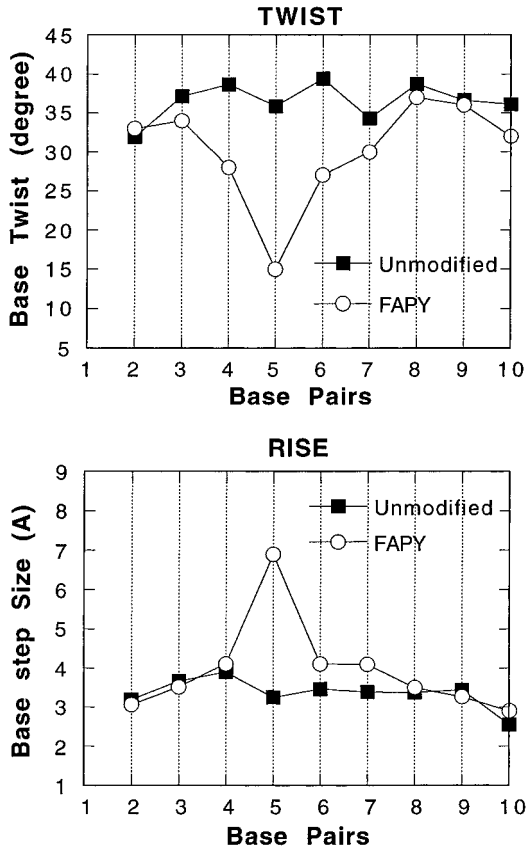

FIGURE 11: Comparison of base twist and base step between the unmodified and AFB_1−FAPY-modified oligonucleotide.

Table 3: Root Mean Square (rms) Deviations, Excluding the Terminal Base Pairs, between the Initial Structures, the Various rMD Structures, and Final Average Structures of the AFB_1−FAPY-Modified Oligodeoxynucleotide

	atomic rms difference (Å)
initial structures	
FAPY−Ai vs FAPY−Bi	5.73
rms shifts	
FAPY−Ai vs ⟨rMD FAPY−Ai⟩[a]	4.23 ± 0.32
FAPY−Bi vs ⟨rMD FAPY−Bi⟩[b]	0.86 ± 0.12
rms distributions	
⟨rMD FAPY−Ai⟩ vs ⟨rMD FAPY−Ai⟩	0.84 ± 0.15
⟨rMD FAPY−Bi⟩ vs ⟨rMD FAPY−Bi⟩	0.76 ± 0.14
⟨rMD FAPY−Ai⟩ vs ⟨rMD FAPY−Bi⟩	0.93 ± 0.25
⟨rMD FAPY−Ai⟩ vs rMD[c]	0.86 ± 0.18
⟨rMD FAPY−Bi⟩ vs rMD	0.73 ± 0.14

[a] ⟨rMD FAPY−Ai⟩ represents the set of six structures which emerged from MD calculations starting with rMD FAPY−Ai. [b] ⟨rMD FAPY−Bi⟩ represents the set of six structures which emerged from MD calculations starting from FAPY−Bi. [c] rMD represents the average minimized structure from all 12 MD calculations.

T^7•A^{14}. In contrast, complete broadening of the imino protons occurred at 50 °C in the unmodified duplex. The stabilization of the T^7•A^{14} base pair was surprising, since it is 2 base pairs downstream of the FAPY adduct. The remarkable stabilization of 4 base pairs is believed to result from a combination of enhanced stacking interactions between T^4•A^{17}, the AFB_1 moiety, and $^{FAPY}G^5$•C^{16}, and on the 3′-side of the lesion, from stabilization of base pair A^6•T^{15} by hydrogen bond formation between A^6 $N6H_a$ and AFB_1 CHO, which holds T^7•A^{14} in place also. This observation correlated with the downfield chemical shift for T^7 N3H of 0.15 ppm, which was consistent with stronger hydrogen bonding of the A^6•T^{15} and T^7•A^{14} base pairs. This hydrogen bond suggests that the both the physical properties and the biological processing of the FAPY lesion may depend upon the DNA sequence.

Structure−Function Relationships. The biological relevance of this structure remains to be determined. The present results suggest that both this stable form of the FAPY adduct and the initially formed cationic adduct are intercalated into the DNA duplex. On this basis, one might predict the processing of the two lesions would be similar. However, despite apparent similarities in structure, the increased thermal stability and the hydrogen bond formation between $^{FAPY}G^5$ CHO and A^6 $N6H_a$ in the FAPY adduct could result in significant differences in lesion processing *in vivo*. Furthermore, the positively charged guanine base in the initially formed cationic lesion and the neutral pyrimidine moiety in the FAPY adduct possess differing electronic and hydrogen bonding properties. Of particular interest is the possibility that the cationic adduct may bend the DNA duplex, which perhaps makes it more recognizable to repair enzymes. In *E. coli*, both the cationic and FAPY−AFB_1 lesions were processed similarly by uvrABC (*44*). In contrast, the FAPY lesion was persistent in rat liver (*18*), suggesting its greater resistance to repair, and giving basis

Table 4: Comparison of Sixth Root Residual Indexes, R_1^x ($\times 10^2$), for Starting Models and Resulting MD Structures[a,b,c]

	intranucleotide R_1^x	internucleotide R_1^x	overall R_1^x
FAPY−Ai	9.5	12.1	11.5
FAPY−Bi	8.8	9.9	8.9
⟨MDA⟩	8.6	9.5	8.7
⟨MDB⟩	8.5	9.4	8.6
⟨rMDav⟩	8.5	9.5	8.7

[a] Only the inner 8 base pairs were used in the calculations, to exclude end effects. The mixing time was 350 ms. [b] $R_1^x = \sum|(a_o)_i^{1/6} - (a_c)_i^{1/6}|/\sum|(a_o)_i^{1/6}|$, where a_o and a_c are the intensities of observed (non-zero) and calculated NOE cross-peaks. [c] FAPY−Ai, starting energy-minimized A-DNA with the AFB_1 moiety intercalated between base pairs 4 and 5; FAPY−Bi, starting energy-minimized B-DNA with the AFB_1 moiety intercalated between base pairs 4 and 5; ⟨MDA⟩, average of 6 rMD structures starting from FAPY−Ai; ⟨MDB⟩, average of 6 MD structures starting from FAPY−Bi; ⟨rMDav⟩, average of 12 rMD structures starting from FAPY−Ai, FAPY−Bi.

to the notion that the FAPY lesion may be of greater mutagenic significance.

It will be of interest to compare site-specific mutagenesis for the cationic and FAPY adducts. Site-specific mutagenesis on the cationic AFB_1 lesion in the sequence context 5′-d($C^{AFB}GA$)-3′ (*45*) revealed the predominant mutation to be GC→TA, consistent with earlier studies (*46*, *47*). The site-specific approach distinguished GC→AT transversions induced by the cationic lesion from those induced by depurination of the N7 adduct. These transversions were dependent on *mucAB* while those derived from the corresponding apurinic site were dependent upon *umuDC*. This supported the contention that the *trans*-8,9-dihydro-8-(N7-guanyl)-9-hydroxyaflatoxin B_1 lesion was responsible for GC→AT transversions. Approximately 13% of the AFB_1-induced mutations were targeted at the cytosine 5′ to the lesion site. This asymmetry was consistent with NMR data in which the cationic AFB_1 moiety was intercalated on the 5′-side of the modified guanine.

That the initially formed d(CTAT^{FAPY}GATTCA)-3′•5′-d(TGAATCATAG)-3′ slowly converted to a single species amenable for structural analysis suggested that the structure refined in the present work represents the energetically most stable form of AFB_1−FAPY in this duplex. Substantial effort is now being made to identify the species initially present in the d(CTAT^{FAPY}GATTCA)-3′•5′-d(TGAATCATAG)-3′ duplex, since the less stable structure might lead to a different biological response than does the structure identified in the present work (*48*). The term "mutagenic switch" was introduced to describe a potential situation in which one of two adduct conformations was mutagenic and the other not, or two conformations potentially leading to differing mutations (*49*).

In summary, the AFB_1 moiety in this AFB_1−FAPY adduct intercalates from the major groove above the 5′-face of $^{FAPY}G^5$, reminiscent of the 5′-intercalation of the corresponding cationic guanine N7 adduct, but with substantially

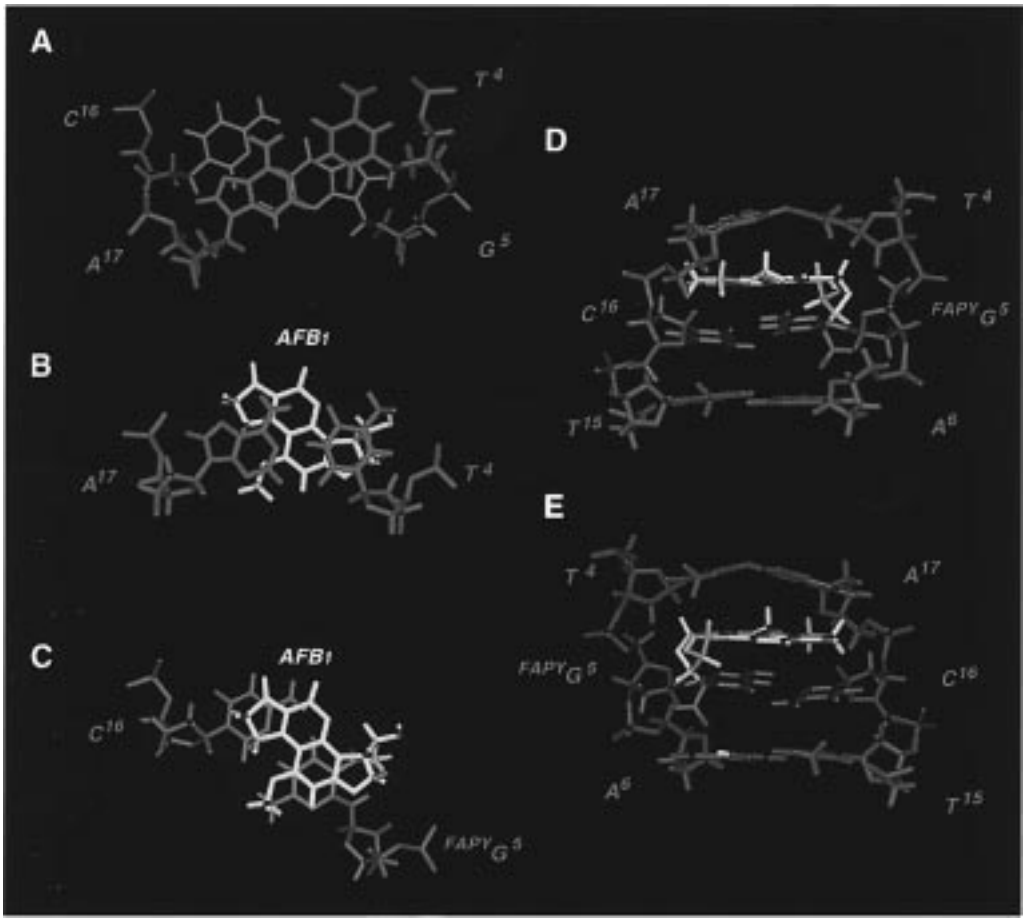

FIGURE 12: Stacking patterns of the AFB_1 moiety relative to DNA base pairs. (A) Base pairs T^4•A^{17} (colored in blue) and G^5•C^{16} (colored in red) for the unmodified duplex. (B) The AFB_1 moiety (colored in yellow) and T^4•A^{17} (colored in blue). (C) The AFB_1 moiety and $^{FAPY}G^5$•C^{16} (colored in red). (D) A side view from the major groove of the adducted site (the formyl proton is colored in green). (E) A side view from the minor groove of the adducted site.

increased thermal stability. This stability is attributed to strong stacking interactions, and to a sequence-specific hydrogen bond between the carbonyl oxygen of the formyl group and the amino proton of the 3′-neighboring adenine. In addition to the chemical stability of this FAPY adduct which may make it an important mutagenic species, increased thermal stability may also contribute to its biological processing.

ACKNOWLEDGMENT

We thank Mr. Markus Voehler for assistance with the collection of NMR data, and Ms. Mary Kerske for assistance with preparation of the manuscript.

SUPPORTING INFORMATION AVAILABLE

Tables 1S−3S detail the assignments of the FAPY-modified and unmodified duplexes. Table 4S shows partial charges calculated for the FAPY lesion. Figure 1S shows stereoviews of the starting structures used in the MD refinements (12 pages). Ordering information is given on any current masthead page.

REFERENCES

1. Qian, G.-S., Ross, R. K., Yu, M. C., Yuan, J. M., Gao, Y. T., Henderson, B. E., Wogan, G. N., and Groopman, J. D. (1994) *Cancer Epidemiol. 3*, 3−10.
2. McCann, J., Spingarn, N. E., Koburi, J., and Ames, B. N. (1975) *Proc. Natl. Acad. Sci. U.S.A. 72*, 979−983.
3. Busby, W. F., Jr., and Wogan, G. N. (1984) in *Chemical Carcinogens* (Searle, C. E., Ed.) pp 945−1136, American Chemical Society, Washington, DC.
4. McMahon, G., Davis, E. F., Huber, L. J., Kim, Y., and Wogan, G. N. (1990) *Proc. Natl. Acad. Sci. U.S.A. 87*, 1104−1108.
5. Groopman, J. D., Cain, L. G., and Kensler, T. W. (1988) *CRC Crit. Rev. Toxicol. 19*, 113−145.
6. Wogan, G. N. (1992) *Prog. Clin. Biol. Res. 374*, 123−137.
7. Bressac, B., Kew, M., Wands, J., and Ozturk, M. (1991) *Nature 350*, 429−431.
8. Hsu, I. C., Metcalf, R. A., Sun, T., Welsh, J. A., Wang, N. J., and Harris, C. C. (1991) *Nature 350*, 427−428.
9. Soman, N. R., and Wogan, G. N. (1993) *Proc. Natl. Acad. Sci. U.S.A. 90*, 2045−2049.
10. Ueng, Y. F., Shimada, T., Yamazaki, H., and Guengerich, F. P. (1995) *Chem. Res. Toxicol. 8*, 218−225.
11. Baertschi, S. W., Raney, K. D., Stone, M. P., and Harris, T. M. (1988) *J. Am. Chem. Soc. 110*, 7929−7931.
12. Johnson, W. W., Harris, T. M., and Guengerich, F. P. (1996) *J. Am. Chem. Soc. 118*, 8213−8220.
13. Gopalakrishnan, S., Byrd, S., Stone, M. P., and Harris, T. M. (1989) *Biochemistry 28*, 726−734.
14. Iyer, R. S., Coles, B. F., Raney, K. D., Thier, R., Guengerich, F. P., and Harris, T. M. (1994) *J. Am. Chem. Soc. 116*, 1603−1609.
15. Essigmann, J. M., Croy, R. G., Nadzan, A. M., Busby, W. F., Jr., Reinhold, V. N., Buchi, G., and Wogan, G. N. (1977) *Proc. Natl. Acad. Sci. U.S.A. 74*, 1870−1874.
16. Hertzog, P. J., Smith, J. R. L., and Garner, R. C. (1982) *Carcinogenesis 3*, 723−725.
17. Groopman, J. D., Croy, R. G., and Wogan, G. N. (1981) *Proc. Natl. Acad. Sci. U.S.A. 78*, 5445−5449.
18. Croy, R. G., and Wogan, G. N. (1981) *Cancer Res. 41*, 197−203.
19. Gopalakrishnan, S., and Patel, D. J. (1993) *J. Am. Chem. Soc. 115*, 9321−9322.
20. Gopalakrishnan, S., Stone, M. P., and Harris, T. M. (1989) *J. Am. Chem. Soc. 111*, 7232−7239.
21. Murray, R. W., and Jeyaraman, R. (1985) *J. Org. Chem. 50*, 2847−2853.
22. Borer, P. N. (1975) in *Handbook of biochemistry and molecular biology*, CRC Press, Cleveland.
23. Piotto, M., Saudek, V., and Sklenar, V. (1992) *J. Mol. Biol. 6*, 661−665.
24. Borgias, B. A., and James, T. L. (1990) *J. Magn. Reson. 87*, 475−487.
25. Arnott, S., and Hukins, D. W. L. (1972) *Biochem. Biophys. Res. Commun. 47*, 1504−1509.
26. Arnott, S., and Hukins, D. W. L. (1973) *J. Mol. Biol. 81*, 93−105.
27. Stewart, J. P. (1983) *Quantum Chem. Prog. Bull. 3*, 43.
28. Schmitz, U., and James, T. L. (1995) *Methods Enzymol. 261*, 3−44.
29. Brunger, A. T. (1992) in *X-Plor. Version 3.1. A system for X-ray Crystallography and NMR*, Yale University Press, New Haven.
30. Brooks, B. R., Bruccoleri, R. E., Olafson, B. D., States, D. J., Swaminathan, S., and Karplus, M. (1983) *J. Comput. Chem. 4*, 187−217.
31. Nilsson, L., Clore, G. M., Gronenborn, A. M., Brunger, A. T., and Karplus, M. (1986) *J. Mol. Biol. 188*, 455−475.
32. Clore, G. M., Gronenborn, A. M., Carlson, G., and Meyer, E. F. (1986) *J. Mol. Biol. 190*, 259−267.
33. Ryckaert, J.-P., Ciccotti, G., and Berendsen, H. J. C. (1977) *J. Comput. Phys. 23*, 327−341.
34. Keepers, J. W., and James, T. L. (1984) *J. Magn. Reson. 57*, 404−426.
35. Ravishankar, G., Swaminathan, S., Beveridge, D. L., Lavery, R., and Sklenar, H. (1989) *J. Biomol. Struct. Dyn. 6*, 669−699.
36. Tomasz, M., Lipman, R., Lee, M. S., Verdine, G. L., and Nakanishi, K. (1987) *Biochemistry 26*, 2010−2027.
37. Boelens, R., Scheek, R. M., Dijkstra, K., and Kaptein, R. (1985) *J. Magn. Reson. 62*, 378−386.
38. Gopalakrishnan, S., Harris, T. M., and Stone, M. P. (1990) *Biochemistry 29*, 10438−10448.
39. Stone, M. P., Gopalakrishnan, S., Raney, K. D., Raney, V. M., Byrd, S., and Harris, T. M. (1990) in *Molecular Basis of Specificity in Nucleic Acid−Drug Interactions* (Pullman, B., & Jortner, J., Eds.) pp 451−480, Kluwer Academic Publishers, Dordrechts, The Netherlands.
40. Gopalakrishnan, S., Liu, X., and Patel, D. J. (1992) *Biochemistry 31*, 10790−10801.
41. Bailey, E. A., Iyer, R. S., Stone, M. P., Harris, T. M., and Essigmann, J. M. (1996) *Proc. Natl. Acad. Sci. U.S.A. 93*, 1535−1539.
42. Beranek, D. T., Weis, C. C., Evans, F. E., Chetsanga, C. J., and Kadlubar, F. F. (1983) *Biochem. Biophys. Res. Commun. 110*, 625−631.
43. Humphreys, W. G., and Guengerich, F. P. (1991) *Chem. Res. Toxicol. 4*, 632−636.
44. Oleykowski, C. A., Mayernik, J. A., Lim, S. E., Groopman, J. D., Grossman, L., Wogan, G. N., and Yeung, A. T. (1993) *J. Biol. Chem. 268*, 7990−8002.
45. Bailey, E. A., Iyer, R. S., Harris, T. M., and Essigmann, J. M. (1996) *Nucleic Acids Res. 24*, 2821−2828.
46. Foster, P. L., Eisenstadt, E., and Miller, J. H. (1983) *Proc. Natl. Acad. Sci. U.S.A. 80*, 2695−2698.
47. Foster, P. L., Groopman, J. D., and Eisenstadt, E. (1988) *J. Bacteriol. 170*, 3415−3420.
48. Broyde, S., and Hingerty, B. E. (1984) *Ann. N.Y. Acad. Sci. 435*, 119−122.
49. Eckel, L. M., and Krugh, T. R. (1994) *Nat. Struct. Biol. 1*, 89−94.

BI9718292